Improved winter conditions in SURFEX-TEB v9.0 with a multi-layer snow model and ice for road winter maintenance

Gabriel Colas[1], Valéry Masson[1], François Bouttier[1], Ludovic Bouilloud[2], Laura Pavan[2], and Virve Karsisto[3]

[1]CNRM, Université de Toulouse,Météo-France, CNRS, Toulouse, France
[2]Météo-France, Toulouse, France
[3]Finnish Meteorological Institute, Helsinki, Finland

Correspondence: Valéry Masson (valery.masson@meteo.fr)

Abstract. Snow-covered or icy roads increase the risk of accidents for drivers, pedestrians, and cyclists. In cities or in remote areas, to prevent these slippery conditions, road winter maintenance decisions are weather-informed by simulations. Numerical road weather models have been developed for this purpose, and mostly built to simulate the road conditions in open environments without shadowing and reflections effects. In this study, we intent to bridge the gap between road weather models and urban climate models to improve cold regions urban modeling and road condition predictions in any environment. We have refined the road surface processes related to winter conditions in the Town Energy Balance (surface externalisée; SURFEX-TEB v9.0), which is an urban climate model used for complex environment modeling. For icy conditions, we have developed an ice content to account for the freezing and melting of the water content on the surface. Additionally, we enhanced TEB's representation of snow on road, previously relying on a single-layer snow model (1-L), with a more precise multi-layer snow model known as Explicit Snow (ES). We have conducted evaluations at two distinct locations: Col de Porte in the Alps and a road weather station in southern Finland. Our findings shows that the enhanced TEB model (TEB-ES) outperforms TEB, as well as two benchmark models, ISBA-Route/CROCUS, and a multiple linear regression in open environments. This results are promising for using TEB to inform road winter maintenance decisions.

1 Introduction

For the past 20 years, meteorological offices in countries impacted by winter conditions have provided road and airport runway weather forecasts to operators during winter maintenance season. These forecasts are valuable to them, as they facilitate the planning of deicing activities, traffic optimization and snow removal. They also facilitate advance planning of preventive measures that should be conducted before the road surface conditions become too dangerous for users. According to Michaelides et al. (2014), the risk of accidents on icy and slippery road is 2-3 times higher than on dry roads. In Sweden, Andersson and Chapman (2010) showed that the accidents were most frequent under winter conditions with road surface temperature below

-3°C and snow-covered or icy road surfaces. Remote areas are the most vulnerable, and even light snowfall can have serious consequences in countries not adapted to these conditions (Vajda et al., 2013). Every year, a significant amount of deicing agents is applied to road surfaces. Pollutants can find their way into natural ecosystems and disrupt the delicate balance of
25 nature. During 2022 in the French Alsace department, 24 000 tonnes of salt have been stored for deicing measures. Also, 500 agents and 121 machines have been rallied for the season (Collectivité Européenne, 2022). Proper utilization of this fleet is essential to maintain road safety across the extensive road network. Thus, the costs associated with dangerous weather conditions in the road sector are significantly higher than those in rail and aviation (Michaelides et al., 2014).

Many factors affect the pavement conditions through various and sometimes complex processes (Qin et al., 2022). Numerical
30 modeling tools are used to monitor surface conditions and plan road maintenance. Physical and statistical models with varying levels of refinement have been developed to accurately predict road conditions. Mostly, road weather forecasts are simulated by Land Surface Models (LSM), but in recent years many statistical models have also been created.

Empirical relationships have been established between the various variables, which influence road conditions. These statistical models often produce satisfactory results with few input variables. They are also easy to implement. Different machine
35 learning algorithms have been used for road surface temperature prediction like simple linear regression (Kršmanc et al., 2013; Sherif and Hassan, 2011), GAM (Yin et al., 2019) or more recently gradient boosting algorithms (Qiu et al., 2020) and neural networks (Yin et al., 2019). Models that directly predict the road conditions, have also been developed with recurrent neural networks (Pu et al., 2022) or random forests methods (Takasaki et al., 2022). Statistical models inherently fail to capture the joint physical evolution of the variables that influence road conditions. They are also considered to have lower performance
40 in complex environments such as urban areas with multiple shading and anthropic effects where physical models can perform better (Lipson et al., 2022). For the reasons described previously, we will focus on heat balance models in this study.

Land Surface Models (LSM) simulate surface variables using the heat balance equation. They can represent various surface types from natural surfaces to urban environment with urban climate models. Mainly used to provide boundary conditions for atmospheric models, LSM surface conditions are key for the prediction of soil-atmosphere fluxes. Many national weather
45 services run land surface models designed to help road winter maintenance. These road weather models focus on integrating various factors affecting the evolution of road conditions(Qin et al., 2022), including the difficult winter road conditions related to snow and ice.

The Canadian road weather model METRo (Crevier and Delage, 2001) and the Norwegian model NORTRIP, (Denby et al., 2013; Nuijten, 2016) predict slippery road conditions with a single shared ice/snow storage content. In Finland, RoadSurf
50 (Kangas et al., 2015) computes two distinct snow and ice reservoirs with a simple approach to the melting of ice and snow on the road. The melting energy is taken into account by using the excess energy to melt the ice and snow instead of warming the road when temperature is above the melting point. In Netherlands, the model takes into account freezing and melting energy (Karsisto et al., 2017). Chen et al (2023) developed a complex formulation for road ice prediction. It computes an explicit one layer water/ice energy equation with complex heat exchanges between the road and the atmosphere. In France, a modified
55 version of the hydrological model ISBA coupled with two multiple multi-layer snow models (CROCUS and ES) was built for road maintenance purposes, (Bouilloud and Martin, 2006; Boone and Etchevers, 2001). The snow model computes prognostic

heat content, water content and density and has been validated on many alpine sites. CROCUS utilization within ISBA-Route leads to accurate road conditions simulations on snow-covered roads (Bouilloud and Martin, 2006).

In urban environments, road weather models fail to accurately model the road surface conditions since specific physical processes are needed to represent the town energetics (Masson, 2000). Simple building-averaged models are able to compute the radiative trapping, surface energy budgets and wind channeling (Masson, 2000). The modeling of urban winter conditions has been little studied in the urban climate community in comparison with summer (Pigeon et al., 2008). Lemonsu et al. (2008) showed that snow-covered urban surfaces contribute to changes in sensible and latent heat fluxes. In an urban climate model (TEB), coupling the road with a simple one-layer snow model leads to improved fluxes in winter (Lemonsu et al., 2010) . Thus, the models SUEWS (Järvi et al., 2014), TEB (Masson, 2000) or Lodz-SUEB (Fortuniak, 2003) include a one-layer snow model to take the effect of snow into account during wintertime. CLMU (Oleson et al., 2010) and JULES (Best et al., 2011) go further and includes a multi-layer snow model over the road.

This study attempts to bridge the gap between urban climate models and road weather models used for road maintenance. On the one hand, as they focus on soil-atmosphere heat exchange, urban models do not include processes relevant to winter road maintenance. On the other hand, road weather models fail to compute accurate road conditions in an urban environment. Some urban climate models bridge part of the gap by including snow and ice accumulation in the road component (Meng, 2017). There are also road weather models that take into account sky-view factors and radiation trapping (Karsisto and Horttanainen, 2023; Denby et al., 2013). Thus, the aim of this study is to improve the representation of winter processes in the TEB urban climate model to make it suitable for winter road operations. A new version of TEB has been developed. It models the challenging winter road conditions associated with snow and ice. Our work presents a new ice storage term and an improved snow model with a multi-layer parametrization (ES) on the road surface.

Section 2 of the paper describes the TEB initial version and the new processes added in the model. Section 3 presents the experimental set up to evaluate the model performance in winter conditions. Section 4 presents the performance of TEB initial version and the new TEB model against measurement at two sites, Col de Porte in France and a road weather station in southern Finland.

2 Methods

2.1 TEB model

The Town Energy Balance Model (TEB) (Masson, 2000) is embedded in the SURFEX software (SURface EXternalisée). The idea of this system was to build a modular system disconnected from an atmospheric model. Rather than being tied to a single atmospheric model, SURFEX can be launched autonomously or coupled to any atmospheric model and it provides surface state variables. It consists of four sub-models that describe different surface types on the globe. Extensively used to study the Urban Heat Island (UHI) in summer, TEB has been validated and incorporated in the Meso-NH model (Lac et al., 2018). Pigeon et al. (2008) performed a winter evaluation of the model on the 2004-2005 Capitoul campaign and showed that the model accurately

simulates surface temperature in cases without snow. Lemonsu et al. (2010) evaluated the one-layer snow model coupled with
90 the road and the roof snow during the Montreal campaign.

TEB is an heat balance model with a local canyon geometry that represents a simplified urban environment. It models two
facing walls separated by a road, as first proposed by Oke et al. (1987), which leads to a fast computation. The TEB model
solves distinct heat equations for each surface (roof, wall and road). The radiative trapping inside the canyon geometry leads
to specific shortwave and longwave energy balance equations forced by the atmosphere for each surface. The net longwave
95 radiation absorbed by each surface is computed between each TEB component interaction. The direct solar flux received by
the road or the walls is computed according to shadowing effects and road direction. The diffuse solar flux is processed using
a sky-view factor and a geometric system for an infinite number of reflections. The following description of TEB is restricted
to the road component as it is the focus of our study.

The ground is discretized with layers of artificial ground representing the road structure and layers of natural soil beneath
100 them. The temperature evolution across all layers is driven by a heat equation that computes the energy stored or emitted
depending on the weather conditions. The road is assumed to be impermeable, so there is no water drainage within the vertical
road layers. Snow and rain intercepted by the soil is confined to the road surface. The snow cover defined as a fraction of the
total road surface p_{nc} divides the road surface. The fraction p_{nc} is computed with the total snowpack water equivalent W_{snow}
(kg m^{-2}) and the parameter $W_{snowmax}$ set to 1kg m^{-2} (Masson, 2000) as :

$$105 \quad p_{nc} = W_{snow}/(W_{snow} + W_{snowmax}) \tag{1}$$

Snow cover fraction p_{nc} that depends on the snow water content, is included in the heat balance equation as :

$$C_{R1}\frac{\partial T_{road}}{\partial t} = (1 - p_{nc}))\frac{1}{d_{R1}}(S_R^* + L_R^* - H_R - LE_R - G_{R1,2}) + p_{nc}\frac{1}{d_{R1}}(G_{Rsnow} - G_{R1,2}) \tag{2}$$

With T_{road} is the road surface temperature driven by the snow-road conduction flux G_{Rsnow}, the conduction flux between
the first and second road layers $G_{R1,2}$, net radiation fluxes S_R^* and L_R^* shown in Fig. 1, and sensible and latent heat fluxes H_R
110 and LE_R. C_{R1} is the road surface heat capacity and d_{R1} the depth of the first road layer.

According to Eq. (2) the TEB road surface energy budget is split according to the snow fraction. Indeed, snow cover insulates
the road surface from the first canyon air layer and vice versa. The snow-covered road surface budget is only driven by the
snow-road conduction term (second right-hand term Eq. (2)). The energy budget on the snow-free fraction of the road is driven
by the latent and sensible turbulent fluxes between the road and the interface canyon air layer, by the radiation absorbed by the
115 road and by the heat conduction from the road sub-layers (first right-hand term Eq. (2)).

The rain is intercepted by the snow-free fraction of the road, and transferred into the available water reservoir W_s at the road
surface in kg m^{-2}. Its maximum capacity W_{smax} in the snow-free fraction is the maximum possible content set to 1 kg m^{-2}
(Masson, 2000). Thus, the evolution equation water for water volumetric equivalent content W_s is :

$$\frac{\partial W_s}{\partial t} = R + R_{melt} - (1 - p_{nc})LE/L_v \qquad\qquad W_s \leq W_{smax} \tag{3}$$

120 where R is the rain rate, R_{melt} represents the snow melting rate (kg m^{-2} s^{-1}), L_v the latent heat of vaporization and LE is the latent heat flux between the road and the lower air layer of the urban canyon. If W_s reaches the maximum capacity available, the excess liquid water leaves the system as runoff.

TEB road surface is coupled with a one-layer snow model (1-L) with an albedo parameterization, and density parameters adjusted for urban environments (Lemonsu et al., 2010). Temperature, water content, density and albedo are solved prognosti-

125 cally and represent the snow layer state at any time. A simple formulation is used for the snow density with an exponential law to represent snow aging. Liquid water melted from snow, R_{melt}, is transferred in the available water reservoir, W_s, or it goes directly into runoff.

2.2 Ice content

To account for icy conditions on the road surface, we model the amount of ice on the road. It is described by the state variable

130 W_i in kg m^{-2}, which represents the liquid water equivalent ice content. W_i evolves by phase-induced changes. First, it interacts with the water content, W_s, by melting and freezing. Second, it interacts with the atmosphere with deposition as shown in Fig. 1.

Several hypotheses are made to best model reality and to be in agreement with the TEB modeling choices. The fraction occupied by ice on the TEB road surface is set to 1 and does not depend on the snow-free fraction. So, the ice layer coexists with the water reservoir, W_s. Contrary to the liquid water content, ice content can grow without any limitation on the part

135 that is not snow-covered. But, when the water content available for freezing is null, the ice content can no longer grow. Also, the ice layer can be snow covered. When the snow covers all the road surface ($p_{nc} = 1$), the existing ice content is insulated from the atmosphere and interacts only by conduction with the road surface. The ice layer under the snow does not interact with the snow layer. As shown in Fig. 1, ice is transparent to the snow-road heat conduction flux G_{Rsnow}. Liquid precipitation is intercepted by the snow-free road fraction and falls directly into the available water content W_s. Thus, the ice-reservoir

140 evolution equation is :

$$\frac{\partial W_i}{\partial t} = F - M - (1 - p_{nc})\frac{LE^*}{L_s} \qquad\qquad W_i \geq 0 \qquad\qquad (4)$$

With F representing the freezing rate (kg.m^{-2} s^{-1}), M the melting rate in (kg.m^{-2} s^{-1}) , p_{nc} the snow fraction on road, L_s the sublimation heat constant and LE^* the solid-gas latent heat flux in W m^{-2}. The freezing rate, the melting rate and the solid-gas latent heat flux are defined by the following equations adapted from Boone et al. (2000):

$$145 \qquad F = \frac{1}{\tau}W_s\frac{\max(O, T_f - T_{road})}{C_l L_f} \qquad\qquad (5)$$

$$M = \frac{1}{\tau}W_i\frac{\max(O, T_{road} - T_f)}{C_l L_f} \qquad\qquad (6)$$

$$LE^* = \gamma_{ice}\rho_a\frac{1}{R_a L_s}[Q_{sati}(T) - Q_a] \qquad\qquad (7)$$

where the triple point temperature is represented by T_f, L_f is the latent heat of fusion of water, R_a the air aerodynamic resistance, ρ_a the air density, τ the characteristic timescale for phase change (3300/0.05 s used in this study), and C_l represents

150 the ice heat capacity thermal inertia coefficient described in Boone et al. (2000). Ice sublimation is assumed to be negligible.

Thus, when the road surface reaches the saturation specific humidity with $Q_{sati}(T) \geq Q_a$, LE^* should be greater than 0, but the term γ_{ice} is set to 0. Otherwise when $LE^* \leq 0$, γ_{ice} is set to 1 and deposition as frost on the road can occur. The melting and freezing process couples the evolution of the ice and water contents. Thus, the water-reservoir evolution equation becomes :

155
$$\frac{\partial W_s}{\partial t} = R + R_{melt} - (1 - p_{nc})LE/L_v - F + M \tag{8}$$

With F, M the freezing and melting rates.

Freezing of water is an exothermic reaction while melting is endothermic. This will affect the energy balance at the surface of the road as shown in Fig. 1. Ice on the roads also changes the exchange coefficient, based on the aerodynamical resistance, resulting in modified turbulent exchange between the road and the first air layer in the canyon. For this process, we suppose
160 that the ice is at the first road layer temperature and the aerodynamical resistance is the same as the one for water.

This process is added to the heat-balance equation as follows :

$$\frac{\partial T_{road}}{\partial t} = \frac{1}{d_{r1}}((1 - p_{nc})LE^* - (F - M)L_v) \tag{9}$$
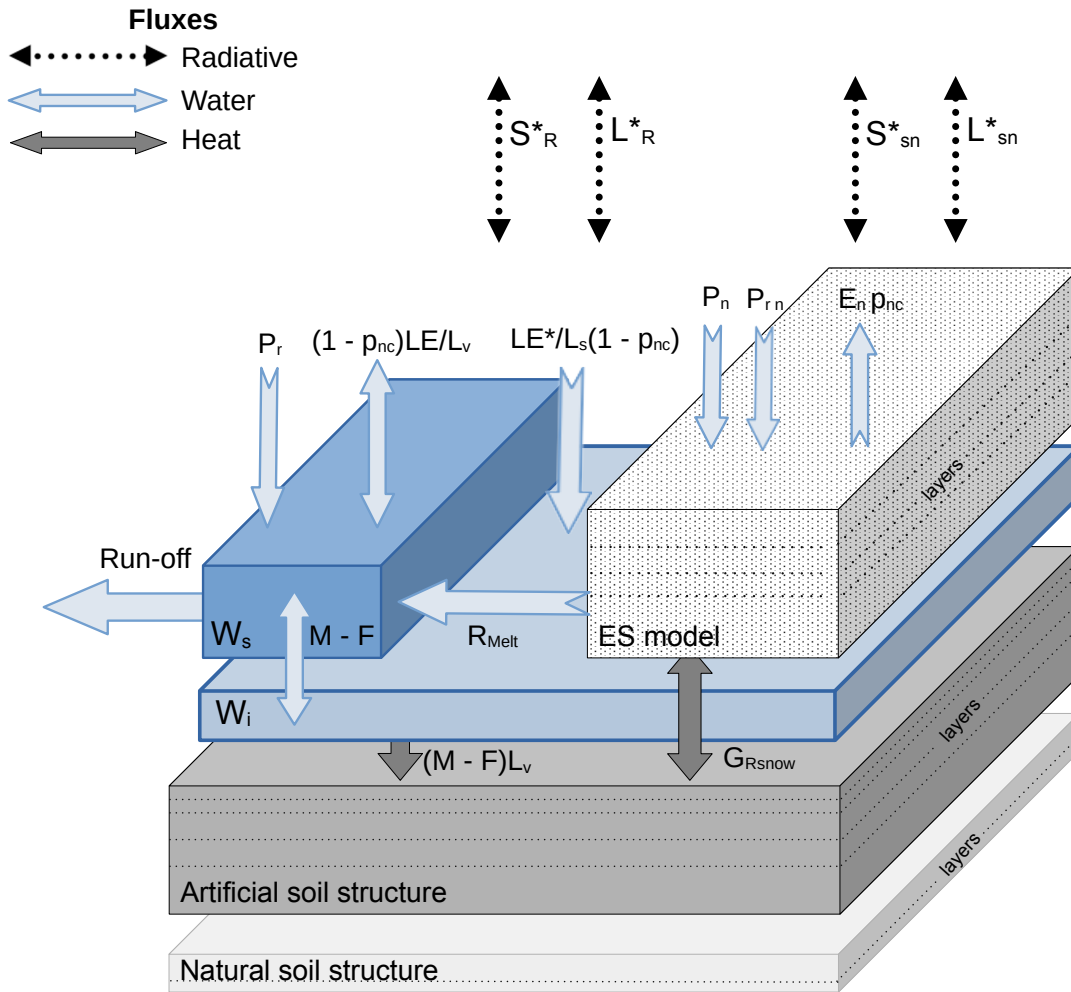
Figure 1. Schematic implementation of the ice content W_i in light blue, the ES model in white and their interaction with the road surface in grey and the water content W_s in blue. Heat, water and radiation effects are represented by arrows with radiative fluxes S^*_{sn} and L^*_{sn} respectively net shortwave and net longwave over snow.

2.3 Explicit Snow model coupling

The snow mantle thermal and liquid profiles cannot be represented by averaged single-layer variables used by one-layer snow model schemes, but require multi-layer models instead (Vionnet et al., 2012). Cristea et al. (2022) showed that numerous layers in snow models increase the performance of the heat change and liquid transfer between the snow mantle layers. Decharme and al. (2016) have also shown that the same snow model with 5-layers rather 3-layers leads to a more accurate soil temperature

evolution. Explicit Snow (ES) (Decharme et al., 2016) is a multi-layer snow model that resolves explicitly the heat-energy balance. The prognostic variables are snow density, heat content, thickness for each snow layer and albedo. To solve a proper

170 snow thermal profile there should be at least 3 layers in the model. Mass and heat are conserved to an high degree of accuracy in the model.

In this work, ES simulates the snow mantle evolution on a road modeled inside the local canyon geometry of TEB. The snow model is forced by the TEB variables. ES receives the computed shortwave radiation from the road sky-view factor and the trapped longwave radiation. It is also forced by the local atmospheric variables computed inside the canyon such as the specific

175 humidity and air temperature. Finally, ES intercepts the snow precipitation and the liquid precipitation. Unlike the one-layer snow scheme (1-L), ES computes the impact of the liquid precipitation on the snow mantle. So, the total liquid precipitation rate R, is split into a fraction that enters the snowpack with P_{rn} (kg m^{-2} s^{-1}) and a fraction that is intercepted by the water reservoir with P_r (kg m^{-2} s^{-1}):

$$P_{rn} = p_{nc}R \tag{10}$$

180 $$P_r = R(1 - p_{nc}) \tag{11}$$

Thus, the water-reservoir evolution equation receives P_r rather than the total liquid precipitation, R in Eq. (8). The snow fraction, p_{nc}, defined Eq. (1), is modified and is set to $p_{nc} = 1$ when the total snow mantle depth D_s is higher than 0.01 m as :

$$p_{nc} = \min(1, D_s/0.01) \tag{12}$$

The atmospheric variables in the TEB canyon are modified by this new snow scheme. For both the 1-L and ES options,

185 the amount of radiation received by the snow-free fraction of the road is weighted by the snow cover. The snow/atmosphere interaction is modified by the ES scheme. The net heat flux, the sensible, latent and radiative fluxes all depend on the local variables inside the snow mantle simulated by ES.

At the bottom of the snow mantle, ES is coupled with the impermeable road surface. Liquid water leaving ES is treated as in 1-L. It is transferred to the water reservoir and then taken into account in the road surface energy balance or leaves the system

190 as runoff. However, the heat conduction between the road surface and the lower snow layer (G_{Rsnow}) is not treated as in 1-L. ES scheme is implicitly coupled to the road surface following the procedure of Masson et al. (2009), to improve stability. Heat conduction between 1-L and the road component heat equations is strictly explicit. It impacts the road surface energy balance as in Eq. (2).

The mass conservation equation for the total snowpack in TEB-ES is :

195 $$\frac{\partial W_{snow}}{\partial t} = P_n + P_{rn} - R_{melt} - E_n \tag{13}$$

W_{snow} is the product of the average snowpack density and the total thickness. It corresponds to the total snowpack water equivalent (SWE) (kg m^{-2}). P_{rn} is the liquid precipitation rate defined Eq. (10), P_n the snow rate, R_{melt} (kg m^{-2} s^{-1}) the melt rate and E_n (kg m^{-2} s^{-1}) the total latent heat flux caused by evaporation and condensation.

Instead of 1-L, each ES layer is characterized by a liquid water content of the snow W_{li}. Index i refers to the layer. It is
modeled as a series of bucket-type reservoirs and the total liquid water content stays $< 10\%$ of the total snow mantle mass
represented by W_{limax} with:

$$\frac{\partial W_{li}}{\partial t} = R_{li-1} - R_{li} + \frac{F_{si}}{L_f} \tag{14}$$

with the condition $W_{li} < W_{limax}$ and:

$$R_{l0} = P_{rn} - (1 - \chi_1)E_n \tag{15}$$

Where R_{li-1} and R_{li} is the water flow between the layers i-1 and i (kg m^{-2} s^{-1}), F_{si} the phase change heat flux (W m^{-2})
that represents the sum of two terms, the available energy for snow to melt and the available energy for the liquid water to
freeze, R_{l0} the flux at the snow surface and χ_1 the fraction of the total mass of the surface layer which is frozen defined as :

$$\chi_1 = 1 - \frac{W_{l1}}{W_{snow1}} \tag{16}$$

The snow-layer density prognostic variable ρ_{si} (kg m^{-3}), changes because of few factors such as the weight of the overlying
snow, the settling mainly due to fresh snowfall, the thermal metamorphism and the snow viscosity. Also, the fresh snowfall
usually reduces the uppermost layer density and is defined as :

$$\rho_{new} = a_{sn} + b_{sn}(T_a - T_f) + c_{sn}(V_a)^{1/2} \tag{17}$$

Where T_a is the air temperature inside the canyon in Kelvin, V_a the wind speed, and coefficients $a_{sn} = 109$ kg m^{-3}, $b_{sn} = 6$
kg m^{-3} K^{-1} and $c_{sn} = 26$ kg. Melting, infiltration of rainwater and retention of snow melt also affect the snow layer density
as described in Boone et al. 2001.

The snow mantle is slightly transparent to the solar radiation flux. The snow mantle's heat balance equation is modified at
each layer by this positive heat flux. The solar transmission heat flux is an negative exponential of the snow depth and the
extinction coefficient for shortwave radiation products. This flux is weighted by the snow surface albedo.

In ES, the snow surface albedo process is adjusted for natural environments and computed as in Decharme et al. (2016). The
impact of human activity, such as pollution sources, on the whiteness of snow is not considered. Thus, the albedo equation and
parameters used in 1-L from Lemonsu et al. 2008 are used in replacement. It impacts directly the solar radiation transmission
heat flux.

3   Experimental set up and assessment

3.1   Model configuration

This study compares the TEB model released in SURFEX v9.0 with the modified version called TEB-ES in published in the
repository (Colas, 2024), that includes the snow and ice related processes described above. Both models are initialized with the

same shared configuration in order to evaluate the impact of the new processes. Two benchmark road weather models are set up and compared to TEB and TEB-ES performance. First, the heat-balance model described in Bouilloud and Martin (2006) named ISBA-Route/CROCUS, which is in operation in the French national meteorological office with a downgraded version is used in comparison. CROCUS is a more complex snow model than ES and is coupled to the surface of ISBA-Route. CROCUS and ES share many similarities, but CROCUS can explicitly calculate snow metamorphism, including grain size and shape evolution, which impact the mechanical properties and albedo of the snow mantle (Vionnet et al., 2012). Secondly, a simple statistical model described in Kršmanc et al. (2013) that is built with a multiple linear regression method (MLR) is used to predict road surface temperature. Simple empirical models are valuable for assessing the need to construct complex physical models for predicting surface variables (Lipson et al., 2024). The best predictive variables for the MLR are found by a stepwise regression procedure that minimizes the root mean squared error. They are chosen among the available forcing variables that are used as input for the heat-balance model described next section. Following Kršmanc et al. (2013), lags of the variables are introduced in the model to help capture the time-varying nature of the physical variables. Thus, input variables have a lag of 3 hours, 2 hours and no lag before the prediction time.

TEB is designed for urban areas but it needs to be adapted for validation sites located in open areas where the pavement is constructed without adjacent structures. The local canyon geometry configuration of the model cannot be completely removed. So, we flatten the canyon geometry to the limit. The canyon aspect ratio was set to 0.0001 which causes the sky-view factor of the road to be close to 1. This nullifies the radiative trapping of the canyon. The building fraction is set to 0.0001 to limit interactions between the air inside the canyon and the TEB building component. With these settings, TEB is considered to simulate a road with open surroundings. The surface boundary layer options is activated and computes explicit atmospheric variables inside the urban canyon (Masson and Seity, 2009) as well as the explicit calculation of the longwave exchanges. We set the pavement structure physical parameters described Table 1 in agreement with Bouilloud and Martin (2006) for a French highway. The natural soil under the artificial structure is initialized in TEB by the dry soil thermal, whereas for TEB-ES it is initialized with the moist soil thermal conductivity (Bouilloud and Martin, 2006). For the second experiment in this paper, the TEB-Hydro component is enabled to simulate water wear-off on the roads (Bernard et al., 2020), and $W_{snowmax}$ is set to 0.6 kg m^{-2} rather than 1 kg m^{-2} to take into account the road properties.

3.2 Experiments

The models are mainly forced by the on-site measurements at the experiment set-up location. They are first assessed at the Col de Porte Météo-France measurement site. Located at an altitude of 1325m in the Chartreuse mountain range in the Alps (45.30° N, 5.77° E), this site, in a grassy meadow surrounded by a coniferous forest, is covered by snow several months a year. In operation since 1959, the Col de Porte Météo-France site is equipped with standard meteorological and snow mantle sensors (Morin et al., 2012). It is a European reference for the study of snow-covered surfaces thanks to the meteorological conditions and its collection of sensors. Thus, data from this site has been exploited to validate many snow models (Decharme et al., 2016; Vionnet et al., 2012; Cristea et al., 2022) and even used for large snow model intercomparison projects (Etchevers et al., 2004). During 3 winters (1997/98-1999/2000), the Col de Porte hosted a large experiment to study the snow-road interface from the

Soil material	Concrete	Natural soil
Number of layers	9	3
Discretization [m]	[0.001 ,0.01 ,0.05 ,0.10 ,0.15 ,0.20 ,0.30 ,0.60 ,1.00]	[1.50 ,2.00 ,3.00]
Soil thermal conductivity [$W.m^{-2}$]	2	1.5 (TEB-ES), 0.5 (TEB)
Dry specific capacity [$J.m^{-2}$]	1840000	1940000
Surface albedo	0.1	n/a
Surface rugosity [m]	0.005	n/a
Surface emissivity	1.	n/a

Table 1. Road configuration and parameters in TEB and the modified model TEB-ES

GELCRO project (Muzet et al., 2000). Six experimental artificial pavements (2m x 3m) shown in Fig. 2 were installed at the site(Bouilloud and Martin, 2006). Road surface temperature and snow depth were monitored on each artificial pavement. The snow cover was frequently cleared by an operator throughout the entire experiment. This experience is a reference to study the snow evolution on roads. It has been used to evaluate the model operating in France (Bouilloud and Martin, 2006), which is

265 our heat-balance road weather model benchmark for this study.

TEB-ES is assessed and compared with TEB, ISBA-Route/CROCUS and MLR. The heat-balance models are forced hourly by the local atmospheric measurements at the static meteorological station. The 6min precipitation measurements are aggregated every full hour to give a precipitation intensity. The type of precipitation is divided by assuming rainfall when the air temperature is > 1°C and snowfall when the air temperature is <= 1°C as done in Bouilloud and Martin 2006. For the other

270 atmopsheric measurements, the value closest to the whole hour is considered. The hourly surface observations provides validation data for the models. The models are evaluated with the experimental artificial pavement equivalent to a French highway surface observations only. Finally, snow depth and ice content are reset to 0 in the models after operator snow removal.

Next, a site with recurring snowy and ice road conditions outside of controlled experimental conditions was selected to assess the models. In southern Finland these kinds of conditions are normal in winter and temperature crosses zero degrees multiple

275 times during the winter season, which makes the surface condition forecasting a challenge. Fintraffic has installed numerous road weather stations to monitor road surface temperature and road conditions. The stations are manufactured by Vaisala and they usually measure road surface temperature with asphalt embedded sensors. Many stations also have optical instruments that measure water, ice, and snow layer thickness. Anthropic effects such as traffic and winter maintenance directly influence the physical variables. The surface temperature and layer thicknesses can vary greatly depending on which part of the road they are

280 measured. For instance, snow compaction by the traffic can drop the snow depth and lead to measurements errors. In addition, the optical sensor might only see the top of the snow or ice layer and is unable to measure the actual thickness. For these reasons, the quantities measured by optical sensor should not be treated as absolute truths but as approximate measurements. They can still be used in the qualitative validation of the models. Among several stations with the most sensors, the Salo Hajala

road weather station (60.435°N, 22.969°E) shown in Fig. 3 has been arbitrarily selected. It is called from now on just "Hajala"
285 for simplicity.

To force and validate the model, we used data from a study conducted by Karsisto and Loven 2019. The used data were
observed variables at Hajala road weather station. Wind speed, air temperature, humidity and precipitation were used as at-
mospheric forcing in the model and processed in the same way as the Col de Porte forcing. Surface measurements including
road surface temperature, water/ice contents, Snow Water Equivalent (W_{snow}) and road conditions were used to validate the
290 models. The hourly atmospheric forcing for the model consisted of a mix of observation data and ERA5 reanalysis. Shortwave
and longwave radiation were extracted from ERA5 at the closest grid point (Hersbach et al., 2020). The studied period was
from October 2017 to May 2018.
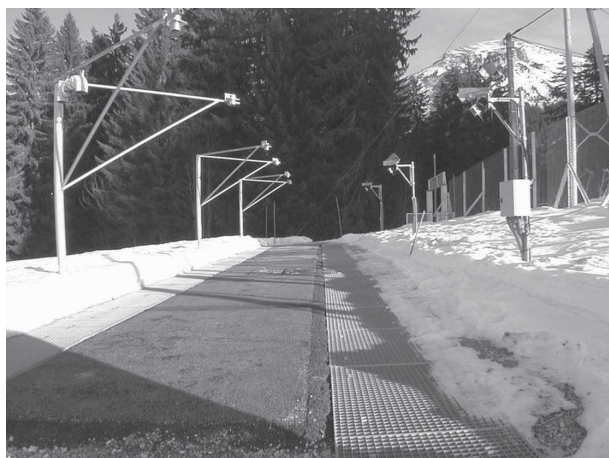
Figure 2. Col de porte experimental artificial soil during
the GELCRO campaign, extracted from (Bouilloud and
Martin, 2006)

Figure 3. Salo Hajala road weather station in Finland,
©Google Steet View 2024

4 Evaluation at the Col de Porte site

First, we compare the performance of TEB, TEB-ES and the benchmarks at the Col de Porte meteorological site during the
295 GELCRO campaign. They are forced by the in-situ measurements and set up to compute the physical variables from 21st

October 1998 6 UTC to 14th May 1999 4 UTC in a continuous simulation over the whole time span. Snow height and road surface temperature are studied on this reference experience for snow-road interface modeling.

4.1 November 7th to 18th period

The time range extracted from the simulation from November 7th to November 18th in Fig. 4 shows typical snow conditions at the measurement site with 5 snow events. During this period, the road was cleared by hand three times. Thus, in the models, on November 13rd at 12h UTC, on November 16th at 11h UTC and on November 17th at 17h UTC, the snow heights and the ice contents are reset to 0. TEB and TEB-ES behaviors are tested and described with 1-L and ES enabled, respectively.

On November 7th, 8th and 9th a synoptic high pressure centered over Western Europe brought calm weather. Conditions were dry with positive air temperature and clear skies. The daily evolution of the road surface temperature is accurately simulated by TEB and TEB-ES. Both simulations are nearly identical, except that TEB-ES has a reduced cold bias during the evening and nighttime. Here, the road surface temperature is driven by road-atmosphere interaction and the pavement conduction. The soil-atmosphere interaction in absence of ice or snow has not been changed for the new TEB version. But the moisture conductivity in the natural soil under the pavement added in TEB-ES as seen in Table 1 leads to improved pavement heat restitution and reduces the cold bias by 0.5 °C.

Several weather perturbations occurred during the following days. The first low pressure system reached the station on November 10th. Rain fell in the afternoon, followed by snow in the evening. TEB-ES simulates lower snow depths than TEB (around 2.7 cm lower for the episode). ES simulates more accurately the heat transfer between the positive road temperature and the fresh snow layers. ES melts almost all snowpack and is closer to the observations as shown in Fig. 4. Therefore the TEB-ES road temperature follows the observations that are driven by the negative air temperature; while TEB road surface temperature is insulated from the atmosphere by the snow mantle. Then, road surface heat change is driven by pavement conduction and snow-road heat transfer. TEB-ES road surface simulation is better than TEB on November 11st and 12nd.

A new shallow low pressure system formed off the coast of Ireland during the November 11st, and narrowed rapidly with weak activity over France on November the 12th. It brought a small amount of snowfall with a snow depth increase during the afternoon of November the 12th. The snow mantle height is well computed by TEB-ES with less than a 2 cm difference with the observations. TEB adds fresh snow to the previous snow mantle on the road and leads to a snow cover 6 cm higher than the measured value.

From the 14th to the 17th of November, a low pressure system persisted over Eastern Europe with several rainfall and snowfall events before a strong ridge brought back high pressure and clear skies. At the beginning of this event, the precipitation forcing is wrong; it was rain rather than snowfall that affected the location. This explains the excessive snow cover in both models. The following snow event is well modeled by both models. ES simulates the fresh snow accumulation more accurately due to the multi-layer parameterization. The mixed composition density of fresh and old snow layers is better represented than in 1-L as described in section 2.3. The temporal evolution of the density of the old snow layer is also better represented with ES (Decharme et al., 2016). Also, road surface temperature is better modeled by ES with a Mean absolute error (MAE) of 0.3 °C and for 1-L a MAE of 1.4 °C during this event. This was a typical isothermal event with a snow-pavement interface layer

330 at constant freezing temperature. This effect is poorly represented by the 1-L snow model that underestimates snow-road heat
transfer.
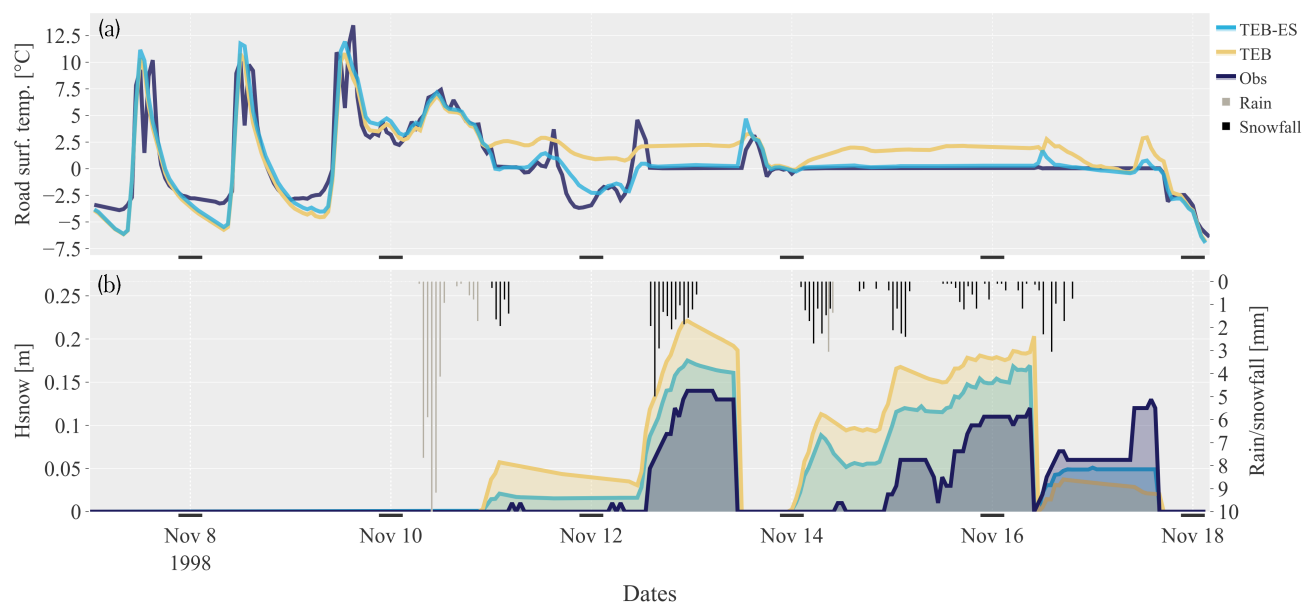
Figure 4. Comparison between the models and the observations at the Col de Porte location. Road surface temperature (modeled and observed) (a), snow height (modeled and observed) and observed rain/snowfall with a reversed y-axis (b)

4.2 Statistical results

Twenty-three snow events occurred during the date range from the October 21st, 1998 at 6 UTC to May 14, 1999 at 4 UTC at the Col de Porte, which is a large enough sample to show statistical differences between the models. Scores displayed in
335 Table 2 show notable differences in the performance of the road surface temperature and snow height simulations. The heat balance models outperform the statistical benchmark. In Table 2, the absence of bias in the TEB road surface temperatures is explained by several biased scores that compensates. Indeed, Fig. 5 shows significant seasonal temperature differences with the observations in TEB. For TEB-ES and ISBA-Route/CROCUS simulations, the seasonal temperature differences with the observations are much lower. TEB-ES's and ISBA-Route's road surface temperatures are more consistent with the observations
340 than the TEB simulation as shown in Table 2 and Fig. 5. Snow height is better simulated by TEB-ES than TEB in terms of RMSE, MAE and R^2 shown in Table 2. Multi-layer snow model coupling greatly improves the snow height and the road surface temperature performance. Because the TEB model is more adapted for man-made structure simulations, validated and calibrated at many locations, it is more accurate than ISBA-Route/CROCUS.

In addition, it is essential to evaluate the ability of the models to capture the occurrence of significant events that could
345 compromise road safety. Table 3 and Table 4 evaluate respectively the capacity of the models to predict potential dangerous

Scores	Snow height [m])			Road surface temp. [°C]			
Models	TEB	TEB-ES	ISBA-Route/CROCUS	TEB	TEB-ES	ISBA-Route/CROCUS	MLR
RMSE	0.19	0.13	0.14	2.82	2.05	2.53	3.64
MAE	0.12	0.08	0.09	2.10	1.33	1.40	2.45
R^2	0.54	0.84	0.80	0.82	0.89	0.83	0.57
Bias	-0.04	-0.02	-0.02	0.02	-0.62	-0.92	0.00

Table 2. Scores for TEB, TEB-ES and the benchmarks (ISBA-Route/CROCUS, MLR) at the Col de Porte location during winter 1998-1999

conditions and snow road condition occurrences. Similar detection rates and missed event rates are found for the models for snow height > 0.5 cm. However, TEB-ES outperforms TEB and ISBA-Route/CROCUS reliability of positive detection with lower false detection and false alarm rates. Surprisingly, TEB outperforms slightly ISBA-Route/CROCUS despite the simple 1-L snow model embedded. During conducive conditions for slippery roads, ISBA-Route/CROCUS has a better detection rate as shown in Table 3 but is less reliable to predict a true negative among all the simulated snow occurrences.

Larger differences in road surface temperature simulations between the heat-balance models are observed in snow-covered isothermal situations. This is is particularly visible during spring 1999 shown in Fig. 5, panel (c), with snow-covered isothermal situations only. In those situations, the TEB road surface temperature is strongly biased, while TEB-ES and ISBA-Route/CROCUS show good performance. ISBA-Route/CROCUS has a slightly better performance than TEB-ES on these situations, due to the complexity of the CROCUS snow model. However, during one particular event in early spring road surface temperature was very poorly simulated by ISBA-Route/CROCUS. These outliers are not shown in Fig. 5. The TEB-ES detection rate is much higher than TEB for road surface temperature < 0.5 °C as shown in Table 3 which can be attributed to snow-covered isothermal situations.

Models	Detection rate %	Missed event rate %	False detection rate %	False alarm rate %
TEB	74	26	4	2
TEB-ES	90	9	5	2
ISBA-Route/CROCUS	97	3	21	9
MLR	70	30	6	4

Table 3. Performance of TEB, TEB-ES and the benchmarks (ISBA-Route/CROCUS, MLR) surface temperature occurrence below 0.5 °C, for 1 hour time step, at the Col de Porte location during the winter 1998-1999

Models	Detection rate %	Missed event rate %	False detection rate %	False alarm rate %
TEB	99	1	18	26
TEB-ES	98	2	16	24
ISBA-Route/CROCUS	98	2	19	27

Table 4. Performance of TEB, TEB-ES and ISBA-Route/CROCUS show depth occurrence greater than 0.5 cm, for 1 hour time step, at the Col de Porte location during the winter 1998-1999
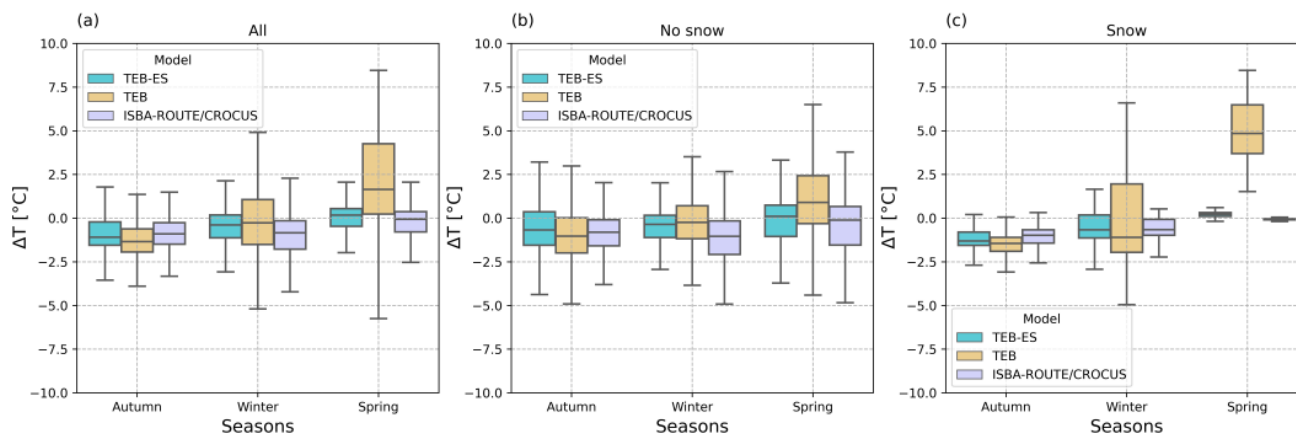
Figure 5. Seasonal road surface temperature differences comparison with the observations between TEB, TEB-ES and the benchmark ISBA-Route/CROCUS. Figures with road conditions partition situations: all cases (a), no-snow observed (b), non zero snow observed (c). The boxes extend from the first quartile (Q_1) to the third quartile (Q_3), with whiskers within $1.5\times$ the interquartile range ($Q_3 - Q_1$).

5 Evaluation at the Hajala site

360   In this section, we take advantage of the detailed observation at the Finnish Salo Hajala road weather station to further validate the physics of the model, in particular, the different mass contents at the road surface. The model is set up to calculate the evolution of the TEB variables for about 6 months in a continuous run, from October 23rd, 2017 at 15h UTC to May the 1st, 2018 at 19h UTC .

5.1   January 17th to 26th 2018 period

365   From January 17th, 2018 to January 23rd, 2018, the Salo Hajala site was affected by a cold air mass with road temperatures below -3°C (Fig. 6). Three small synoptic scale snow events impacted traffic conditions by causing snow cover on the roads. Then, on January 24th the weather regime changed with a low pressure system which brought snowfall, then warmer air with rain.

Small persistent snowfalls on January 17th and January 18th in the morning were induced by a small low surface pressure
370   associated with a weakly active quasi-stationary front. TEB and TEB-ES simulates the appearance of a thin snow cover several hours before the sensor measurement as shown in Fig. 6. This difference could be explained by the high traffic intensity during these hours. The blowing of snow by the traffic removed the thin flake layer on the road and delayed the buildup of the snow cover (Denby et al., 2013). Then, the sensors measured ice and snow simultaneously as the road began to be affected by solid precipitation. This is a common spurious ice detection issue with the sensor. There could be not ice, as the conditions were
375   snowy and there was no liquid water to freeze on the road surface. Both models correctly capture the snow layer evolution. The snow cover is removed by hand at 6 h UTC in the models. The modeled road surface temperatures are consistent with the observed increasing trend during the afternoon of January 18 and show good performance.

On January 19th and 20th, during the nights, the sensor detected liquid water on the road surface. The sky was clear, and the raingauge did not capture any rain. Thus, it is a spurious water detection by the sensor. TEB-ES simulates a possible small
380   hoarfrost event that could have been captured by this sensor.

Both snow simulations match the observed SWE in late evening January 21st. But in January 22nd in the afternoon, the observed contents dropped to 0 mm whereas the simulated SWE's increase. Snow ploughing weekday operations occurred during the day until noon. TEB and TEB-ES simulations are consistent with the observed snowfall and the surface state.

Then, in the night between January 23rd and January 24th, the upstream warm front of the weakening low pressure system
385   brought moderate snowfall. The snow water equivalent evolution by the models matches the observed snowfall. In the morning, snow ploughing and salting removed the snow deposition on the road which we modeled by a simple manual removal of snow cover at 6 h UTC. These operations are largely responsible for the observed water increase. In the afternoon of January 24th, the air temperature rises due to the warmer air mass brought in by the low pressure system. TEB-ES snow melts accordingly whereas TEB the snowpack melts slowly before it is set to zero by the manual removal operation parameterization at 6 h UTC.
390   Finally, the road was wetted by rainfall in the warmer air mass brought by the low pressure system. In the night of January 25th, in clear sky conditions, TEB-ES model correctly captures the freezing of water on the road.
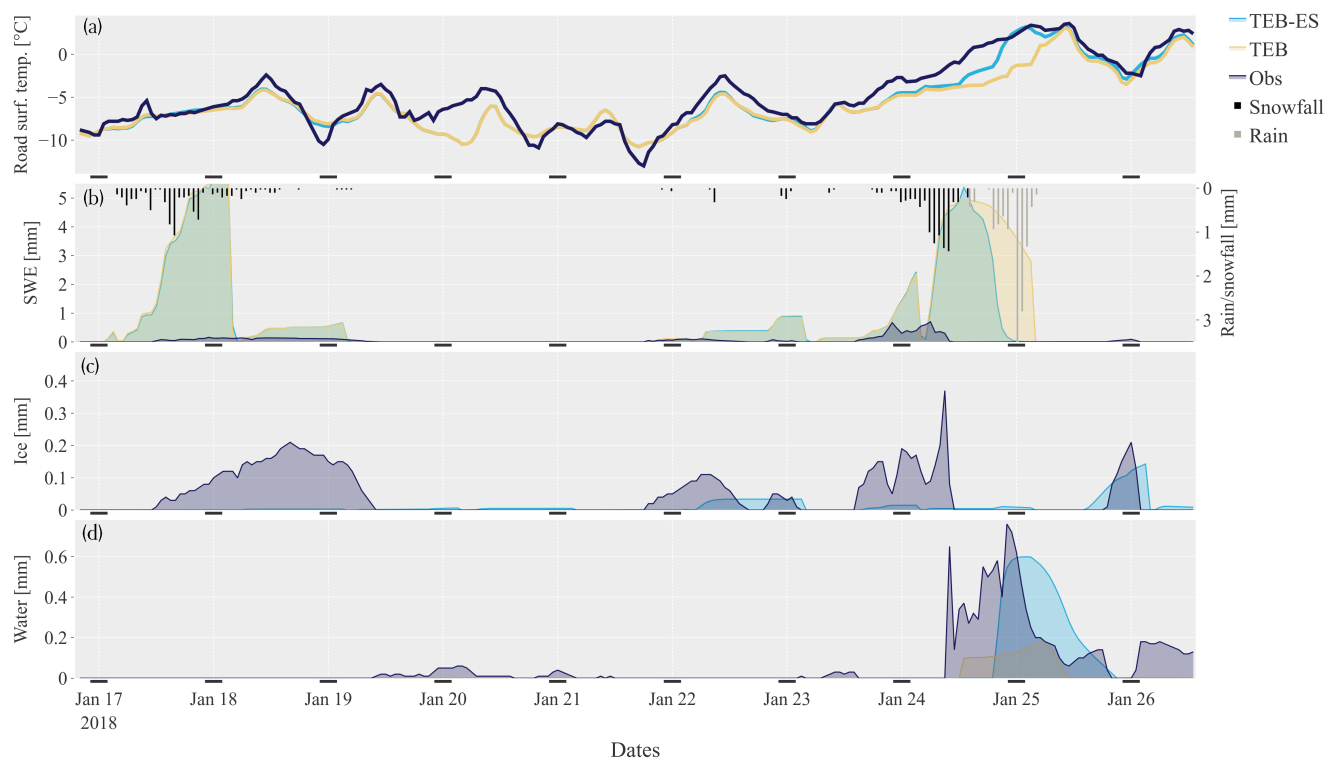
Figure 6. Comparison between TEB, TEB-ES and the observations at the road surface on a road weather station at Hajala. Road surface temperature (modeled and observed) (a), snow water equivalent (modeled and observed) and observed rain/snowfall (b), ice on road (modeled and observed) (c), water on road (modeled and observed) (d)

5.2 April 1st to 7th period

In early April, a low pressure system traveled fast from the Baltic States to Hajala and hit the station with the first snowfall on April 2nd, at 2 h UTC. Uninterrupted moderate snowfall occurred at the station until 14 h UTC from the warm front and then
395 the occlusion of the low pressure system. This standard snow event had probably been anticipated with brine injection during the night since the water content observed increases. Since the salting effect is not modeled, both models poorly simulated the snow water equivalent captured by the Vaisala sensors as shown in Fig.7. However, the overall timing of snow cover is well captured by the models because they use observed precipitations as input.

The road surface temperature is well simulated by both model. The models capture the diurnal cycle of surface temperature in
400 clear sky conditions. They also capture the positive surface temperature with rainy conditions and an overcast sky on April 4th. In snow and ice-free conditions, the simulated water content evolutions are similar. When the road was salted on the morning of April 2th, the more sophisticated modeling in TEB-ES fails to improve the SWE since the salting process is missing to represent these impacts. On April 6th at noon, our precipitation type procedure diagnoses small snowfall instead of rainfall, leading to a

false positive light snow event. The sensors detected a small amount of water on the road. Then, in the early afternoon, the road
405   surface temperature simulated by both models are positive with negative air temperature and snowfall observed. TEB-ES melts
the simulated snowpack quickly, whereas the SWE simulated by TEB remains stable until the parametrized snow removal at 6
h UTC. Clear sky conditions during the same night were cold enough to freeze the water on the road. Later the road was salted,
which melted the ice. TEB-ES water content from the snow mantle melting is frozen and the model accurately reproduces the
observed content on the road which was presumably ice.
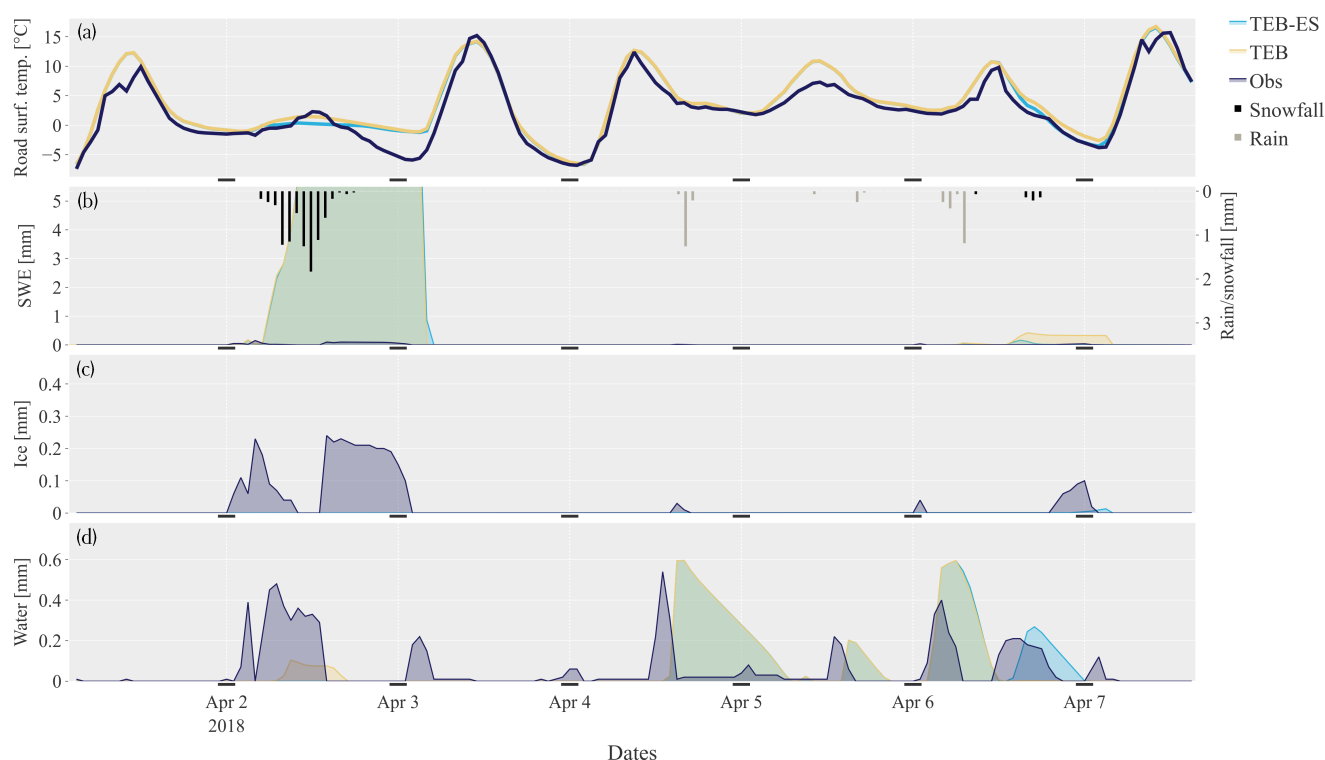
Figure 7. Comparison between TEB, TEB-ES and the observations at the road surface on a road weather station at Hajala. Road surface
temperature (modeled and observed) (a), snow water equivalent (modeled and observed) and observed rain/snowfall (b), ice on road (modeled
and observed) (c), water on road (modeled and observed) (d)

410   **5.3   Statistical results**

Statistical scores are calculated hourly at the Hajala site for the whole simulation. The approach is similar to that used for
the Col de Porte site. Overall TEB and TEB-ES road surface temperature performance shown in Table 5 are almost similar.
TEB-ES is slightly better on RMSE and MAE but does not improve the R^2 and bias. The slight increase in performance is due
to better simulation of the snow cover in the snow-covered situation, as shown Fig. 8. On the panel (c), TEB-ES road surface
415   temperature differences are less spread than TEB and almost centered over 0 °C. Figure 8 reveals a seasonal performance trend

in snow-free situations with all models. The overall temperature differences in spring is higher than in autumn and in winter. In addition, the road surface temperature difference spread is lower in winter in both models.

The snow water equivalent scores are difficult to interpret due to salting. The road lanes are frequently treated with salt and the snow is removed by winter service vehicles. Thus, the observed occurrences of snow cover are much lower than modeled (706 hours observed, 1394 modeled by TEB and 1417 modeled by TEB-ES) and lead to a > 60 % false alarm rate on both models as shown Table 7. Also, the snow occurrence detection by the model shows < 25 % false detection rate and > 70 % detection rate.

Several stacked effects explain the low performance for the ice content variable as shown in Table 8. The optical ice sensor detects ice whenever snow is detected. The measurement recorded 706 occurrences of both ice and snow at the same time. In total, 706 snow occurrences and 743 ice occurrences are measured. Thus, the optical sensor is not able to distinguish between snow-covered or ice-covered road conditions on busy lanes. The other 37 hourly occurrences for ice are at the beginning or at the end of a snow event. This explains the high missed event rate shown in Table 8. In Hajala experiment, around 28 % of the events modeled as ice are observed as water events in non freezing conditions (Road surface temperature measured is $> 0°C$) as illustrated in Fig. 9. Around 96 % of these 28 % events were actually observed as ice-free wet road. This explains the high number of false alarms shown Table 8, which are explained by the cold bias in the model. Freezing occurs more often than observed with 743 ice occurrences observed and 1368 ice occurrences modeled.
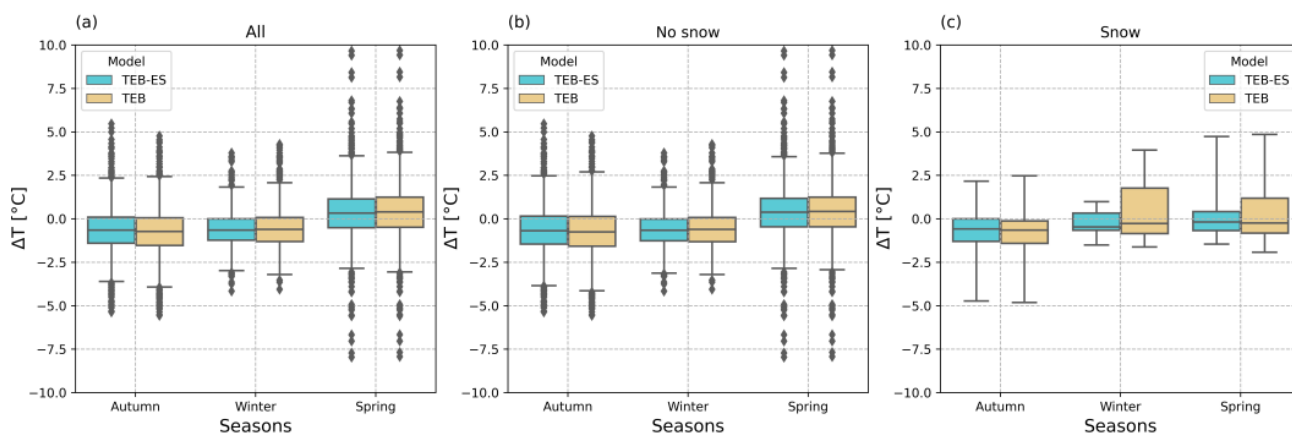
Figure 8. Seasonal road surface temperature differences comparison with the observations between TEB and TEB-ES. Figures with road conditions partition situations: all cases (a), no-snow observed (b), non zero snow observed (c). The boxes extend from the first quartile (Q_1) to the third quartile (Q_3), with whiskers within $1.5\times$ the interquartile range ($Q_3 - Q_1$).
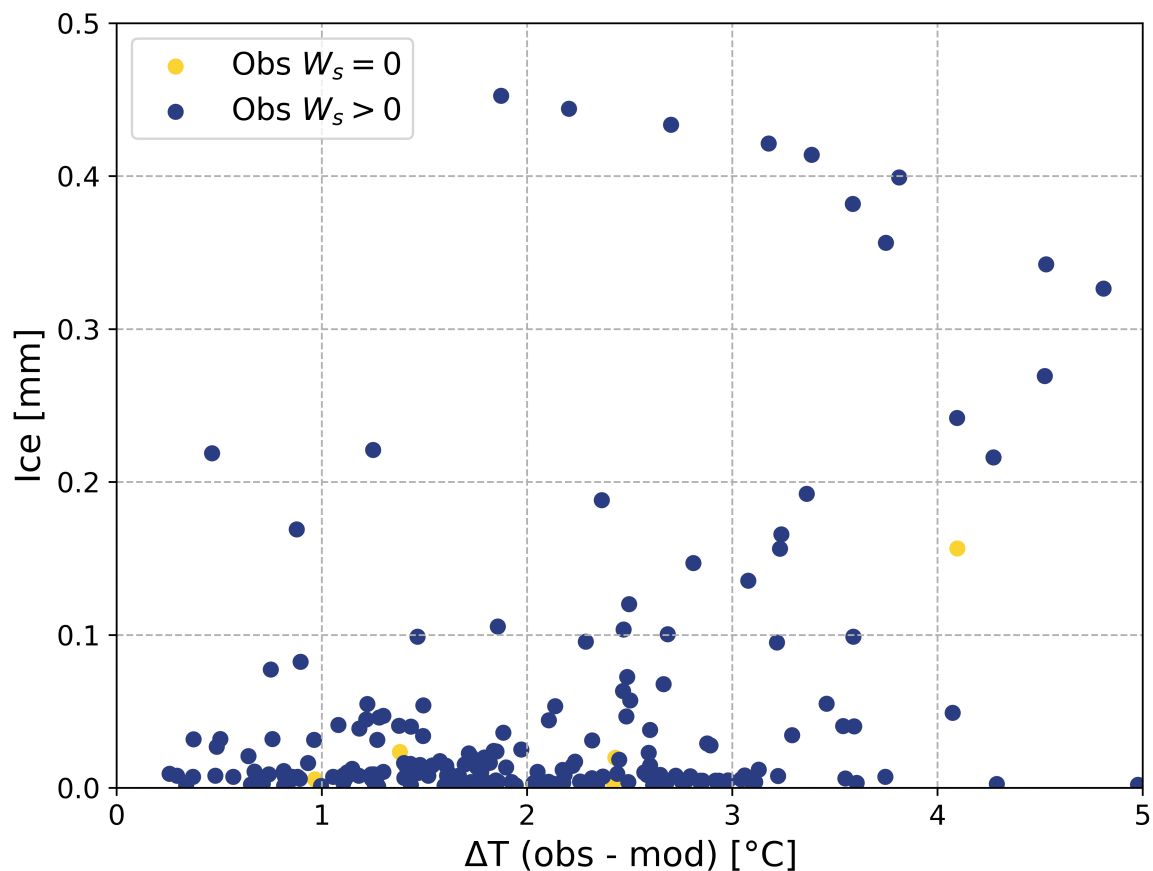
Figure 9. Hourly ice depositions in mm modeled on the road by TEB-ES (with ice depth occurrence greater than 0.001mm); function of the observed and simulated surface temperatures differences $\Delta T (obs - mod)$ when $T_{obs} > 0°C$ and $T_{mod} < 0°C$. The colors shares the points by: observed water content on the road ($Obs\,W_s > 0$) or dry road ($Obs\,W_s = 0$).

6 Discussion

TEB and TEB-ES simulations have demonstrated good performance on the Col de Porte and Hajala experiments, and the model physics are consistent with reality. The urban climate model TEB is well-suited to simulate the surface response to atmospheric

435 variables in man-made structures. When using snow models with similar characteristics, TEB outperforms ISBA-Route in winter conditions. The heat balance models outperform the statistical benchmark. The surface temperature depends on physical variables that can be difficult to observe, such as subsurface temperatures or snow layer properties. Simple relationships with

	TEB	TEB-ES
RMSE	2.51	2.27
MAE	1.19	1.12
R^2	0.95	0.95
Bias	-0.31	-0.31

Table 5. Road surface temperature scores for the Hajala site during winter 2017-2018.

Models	Detection rate %	Missed event rate %	False detection rate %	False alarm rate %
TEB	95	5	18	12
TEB-ES	97	3	18	12

Table 6. Performance of TEB and TEB-ES surface temperature occurrence below 0.5 °C, for 1 hour time step, at the Hajala site during the Winter 2017-2018

atmospheric variables are insufficient to describe this complexity. Therefore, it is useful to develop heat balance models, such as urban models, land surface models, and snow models, for land surface modeling.

440   Overall model performance for the Finland experiment is poorer than for the Col de Porte experiment as shown by the experiment's missed event, false detection and false alarm rates shown in Table 7, Table 6, Table 4 and Table 3. This inferior performance is caused by several factors, including errors in modeling snow removal, anthropic effects not modeled (snow compaction and heating effects by traffic), precipitation not detected by the raingauge, errors in distinguishing between snow and rain, and sensor detection errors. In fact, the traffic has a large effect on snow compaction. It drops the snow depth and

445   leads to measurements errors. Also, Finland's winter road maintenance operator salt major roads whenever any slippery road condition is observed or forecasted. Snow ploughing and salting is roughly simulated in the models by mechanical snow and ice removal every morning at 6h UTC. The actual effects and timings of the winter service vehicles are more complicated and impact the water contents and the surface heat energy. Salting indirectly affects road surface temperature by melting the snow cover that insulates the road from the atmosphere. Indeed, Fig.7 shows that while the large modelled snow depth keeps the

450   road surface temperature steady on April 2nd, the variation of the measured road surface temperature follows the variation of the air temperature.

The seasonal differences in atmospheric forcing impact various processes that influence road surface temperatures and lead to a seasonal road surface temperature performance trend (Fig. 5). During autumn, the road surface temperature increase by the heat conduction from the sub-layers , while in winter, the road surface temperature is driven by the road-atmosphere conduction.

455   In spring, radiative forcing is higher and exhibits pronounced diurnal cycles. Road surface temperature performance differences between TEB and TEB-ES are significant due to the natural soil moisture conductivity initialization. The cold bias on road

Models	Detection rate %	Missed event rate %	False detection rate %	False alarm rate %
TEB	71	29	22	63
TEB-ES	72	28	20	60

Table 7. Performance of TEB and TEB-ES SWE occurrence greater than 0.01 mm, for 1 hour time step, at the Hajala site during the winter 2017-2018

Models	Detection rate %	Missed event rate %	False detection rate %	False alarm rate %
TEB-ES	56	44	25	70

Table 8. Performance of TEB and TEB-ES ice depth occurrence greater than 0.001mm, for 1hour time step, at the Hajala site during the winter 2017-2018

surface temperatures is reduced in TEB-ES by this initialization modification. It increases the heat restitution from the natural soil in winter. That situation is reflected on the November 7th, 8th and 9th 1998 as described in the section above. It also reduces the road surface temperature cold bias when the snow cover insulates the road surface from the atmosphere.

460   The Col de Porte experiment is more reliable to validate the snowpack evolution simulations. The main differences in snow height between TEB and TEB-ES models can be summarized by three processes. First, TEB-ES snow mantle tends to be lower than TEB snow mantle at the beginning of the events. Heat transfer between the pavement and the snow is better represented in TEB-ES. Also, fresh snow properties and accumulation on old snow cover is also better modeled in TEB-ES due to specific density for each layer in the model. Secondly, TEB-ES snow mantle tends to be higher than TEB a few hours

465   after each snowfall. TEB snow density follows a simple formulation with an exponential law to represent snow mantle aging whereas TEB-ES density is affected by weight compaction melting, rainwater infiltration, and snowmelt retention. Thirdly, In snow-covered isothermal situations there are large differences between TEB and TEB-ES. These isothermal situations are common during early winter and spring snowfalls, when the radiative forcing is high. The pavement returns the energy stored in its structure to the snow cover. The lower layers of the snowpack melt, causing liquid water to drain. In ES and

470   CROCUS, the lower snowpack reaches its maximum liquid water content and the snowpack temperatures are at the freezing point. Thus, in TEB with the simple 1-L snow model, snow-soil heat-transfer is underestimated. Overall, the TEB-ES snow height follows the observed trend more closely, as shown by the significantly higher R^2. There are some important differences between the snowpack evolution of TEB-ES and ISBA-Route/CROCUS but the overall snowpack height performance and road surface temperature in observed snow-covered situation as shown are close (Fig 2 - Fig. 5). However, the heat-balance model

475   ISBA-Route is generally more cold biased than TEB and leads to larger false alarm and, false detection rates (Fig. 3, Fig. 4). In one snow-covered event in early spring (not shown here) ISBA-Route/CROCUS has very large error in simulated surface temperature unlike TEB and TEB-ES. This is caused by the different snow fraction formulation between TEB and ISBA-Route.

In this study, the performance evaluation of TEB and its modified version TEB-ES has been carried out in open surrounding areas to investigate whether this urban climate model can accurately reproduce the road conditions predicted by road weather models. The TEB-ES road surface temperature performance shown in this study appears similar to heat-balance road weather models at other locations (Meng, 2017; Nuijten, 2016; Denby et al., 2013). Some of these models have been tested in open environments, while others have been tested in urban areas. TEB has been created to simulate the urban climate and has been successful in modeling urban heat island effects (Suher-Carthy et al., 2023). Further research is needed to evaluate the road condition forecast in complex environment such as facing walls or roadside trees (Lemonsu et al., 2012). TEB is used as well for surface boundary conditions, coupled with research (Lac et al., 2018) and operational (Masson et al., 2013) atmospheric models. Flux modeling assessment for model coupling should be performed as in Lipson et al. 2024. There are some limitations in our winter road condition modeling, in particular in ice content modeling and its evaluation, which could be upgraded with layer temperature evolution as in Chen et al. (2023) or Fujimoto et al. (2014). Missing real-world processes in the models may be a part of the explanation (Eram et al., 2014) for lower peformance in Hajala experiment. The influence of anthropic effects such as traffic and salting are not modeled in TEB and TEB-ES despite its major impact on the snow depth (Fujimoto et al., 2014; Giudici et al., 2019).

7 Conclusions

Bringing together the best of urban climate and road weather models benefits both communities. For the urban climate community, better modeling of winter road conditions can lead to important improvements of heat fluxes in cities where winter conditions are frequent. Of particular relevance to the road weather community, improved modeling of the environment could improve the accuracy of road condition prediction, especially in complex urban environments.

Thus, a modified version of TEB from SURFEX-TEB v9.0 has been developed for winter road conditions. The road surface processes have been enhanced to model hazardous winter driving conditions. We incorporated a basic ice content to depict frost and water freezing on the road and a new, precise, snow model that is coupled with the road. The model's new physics has been verified at two different winter sites. One experiment was conducted under controlled conditions at Col de Porte, while the other was based on a real-world scenario in Hajala, Finland. TEB-ES significantly enhanced the surface condition prediction accuracy for the Col de Porte controlled experiment, outperforming both benchmarks. Periods that are suitable for slippery conditions are well detected in TEB-ES. Thus, during snowfall, the road's snow coverage is accurately simulated. However, Hajala road weather station experiment shown that further developments are needed to account for anthropic effects. Traffic heating, salting, water splashing, and snow compaction impact the road surface conditions and the road surface temperature.

Appendix A: Statistical benchmark model

A Multiple Linear Regression (MLR) is developed in this study for predictive purposes as a benchmark for the Col de Porte experiment. The model is developed using the same knowledge used by the heat-balance models to simulate the road surface

Selected variables with lag	-3 hours	-2 hours	No lag
	Temperature	Temperature	Temperature
	Direct shortwave	Direct shortwave	Direct shortwave
	Specific humidity		Scattered Shortwave
			Longwave

Table A1. Variables used for the MLR model learning and inference

temperature. Thus, the wind-speed, wind direction, solar radiation direct and scattered, longwave radiation, air temperature,
510 specific humidity and pressure forcings are used as input data for the MLR model. Following Kršmanc et al. (2013), the
hourly forcing variables from a lag of 3 hours, 2 hours and no lag are concatenated. In total, 24 explanatory variables are
considered by the model. A backward feature selection procedure is performed to prevent overfitting. The selection is made
using the adjusted-R^2 criterion that unlike the R^2 is not monotonically non-decreasing by the number of explanatory variables.
The selection procedure results are drawn Fig. A1 with cross-validation estimator performance uses. The maximum mean
515 adjusted-R^2 calculated by the selection procedure shown Fig. A1 is used to select the variables needed for the model. The
maximum mean adjusted-R^2 is 0.678 for nine variables extracted shown Table A1. In this paper, the model predictions are
made in-sample. It means that, the data used for inference are also used to learn the model.
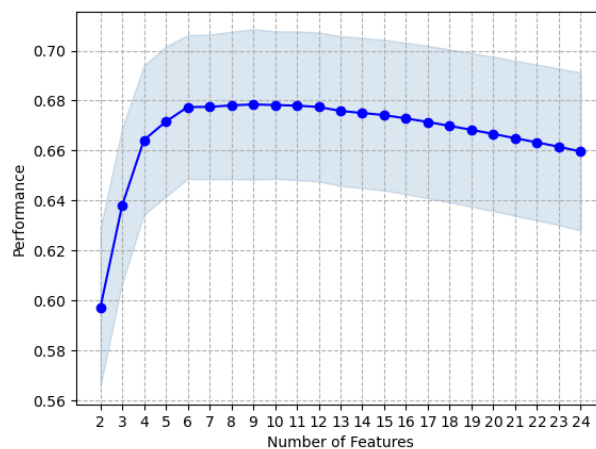
Figure A1. Sequential feature selection performances with 20 cross-validation steps, for the multiple linear regression with the adjusted-R^2 in function of the backward selected features number, with the 0.95 confidence interval

Code and data availability. TEB is embedded in the software *SURFEX* available from the CNRM open source website: https://opensource.
umr-cnrm.fr under the *CeCILL Free Software License Agreement v1.0* license. The exact version of SURFEX v9.0 including the TEB model,

520 the TEB-ES model and the MLR statistical model used to produce the results in this paper, are available for public access on the Zenodo
platform (Colas, 2024), as are the input data to run the models and output data to evaluate all the simulations presented in this paper.
ISBA-Route/CROCUS code is not publicly available because it is not an open-source model.

Author contributions. GC conducted the model improvements and benchmarks, investigation, methodology, formal analysis, validation, data
curation and wrote the paper. VM, FB and LC conceptualized and supervised the project, participated for the methodology, validation, and

525 reviewed the paper. VK has participated in the data curation, validation, and reviewed the paper. LP made a draft of the model improvements
with investigations and validations and reviewed the paper. All authors discussed the performance of the models.

Competing interests. The authors declare that they have no conflict of interest

References

Andersson, A. and Chapman, L.: The use of a temporal analogue to predict future traffic accidents and winter road conditions in Sweden,
    Meteorol Appl, 18, https://doi.org/10.1002/met.186, 2010.

Bernard, E., Chancibault, K., de Munck, C., and Mosset, A.: A new hydro-climate model for urban water management including nature based
    solutions: a preliminary application on Paris metropolitan area, https://doi.org/10670/1.3xuj45, 2020.

Best, M. J., Pryor, M., Clark, D. B., Rooney, G. G., Essery, R. L. H., Ménard, C. B., Edwards, J. M., Hendry, M. A., Porson, A., Gedney, N.,
    Mercado, L. M., Sitch, S., Blyth, E., Boucher, O., Cox, P. M., Grimmond, C. S. B., and Harding, R. J.: The Joint UK Land Environment
    Simulator (JULES), model description – Part 1: Energy and water fluxes, Geosci Model Dev, 4, 677–699, https://doi.org/10.5194/gmd-4-
    677-2011, 2011.

Boone, A. and Etchevers, P.: An Intercomparison of Three Snow Schemes of Varying Complexity Coupled to the Same
    Land Surface Model: Local-Scale Evaluation at an Alpine Site, J Hydrometeorol, 2, 374–394, https://doi.org/10.1175/1525-
    7541(2001)002<0374:AIOTSS>2.0.CO;2, 2001.

Boone, A., Masson, V., Meyers, T., and Noilhan, J.: The Influence of the Inclusion of Soil Freezing on Simulations
    by a Soil–Vegetation–Atmosphere Transfer Scheme, J Appl Meteorol Clim, 39, 1544–1569, https://doi.org/10.1175/1520-
    0450(2000)039<1544:TIOTIO>2.0.CO;2, 2000.

Bouilloud, L. and Martin, E.: A Coupled Model to Simulate Snow Behavior on Roads, J Appl Meteorol Clim, 45, 500 – 516,
    https://doi.org/10.1175/JAM2350.1, 2006.

Chen, J., Sun, C., Sun, X., Dan, H., and Huang, X.: Finite difference model for predicting road surface ice formation based on heat transfer
    and phase transition theory, Cold Reg. Sci. Technol., 207, 103 772, https://doi.org/10.1016/j.coldregions.2023.103772, 2023.

Colas, G.: Datasets and model changes for: Improved winter conditions in SURFEX-TEB v9.0 with a multi-layer snow model and ice for
    road winter maintenance, https://doi.org/10.5281/zenodo.11257609, 2024.

Collectivité Européenne, A.: Le service de déneigement alsacien activé, https://www.alsace.eu/presse/
    le-service-deneigement-alsacien-active/, 2022.

Crevier, L.-P. and Delage, Y.: METRo: A and New Model and for Road-Condition and Forecasting in Canada, J. Appl. Meteorol., 40,
    2026–2037, https://doi.org/10.1175/1520-0450(2001)040<2026:MANMFR>2.0.CO;2, 2001.

Cristea, N. C., Bennett, A., Nijssen, B., and Lundquist, J. D.: When and Where Are Multiple Snow Layers Important for Simulations of
    Snow Accumulation and Melt?, Water Resour. Res., https://doi.org/10.1029/2020wr028993, 2022.

Decharme, B., Brun, E., Boone, A., Delire, C., Moigne, P. L., and Morin, S.: Impacts of snow and organic soils parameterization on northern
    Eurasian soil temperature profiles simulated by the ISBA land surface model, The Cryosphere, 10, 853–877, https://doi.org/10.5194/tc-
    10-853-2016, 2016.

Denby, B., Sundvor, I., Johansson, C., Pirjola, L., Ketzel, M., Norman, M., Kupiainen, K., Gustafsson, M., Blomqvist, G., Kauhaniemi, M.,
    and Omstedt, G.: A coupled road dust and surface moisture model to predict non-exhaust road traffic induced particle emissions (NOR-
    TRIP). Part 2: Surface moisture and salt impact modelling, Atmos. Environ., 81, 485–503, https://doi.org/10.1016/j.atmosenv.2013.09.003,
    2013.

Eram, M., Blomqvist, G., Gustafsson, M., and Thordarson, S.: Residual salt model for daily application in winter ser-
    vice management, https://www.researchgate.net/publication/275647536_RESIDUAL_SALT_MODEL_FOR_DAILY_APPLICATION_
    IN_WINTER_SERVICE_MANAGEMENT, 2014.

565 Etchevers, P., Martin, E., Brown, R., Fierz, C., Lejeune, Y., Bazile, E., Boone, A., Dai, Y.-J., Essery, R., Fernandez, A., Gusev, Y., Jordan, R., Koren, V., Kowalczyk, E., Nasonova, N. O., Pyles, R. D., Schlosser, A., Shmakin, A. B., Smirnova, T. G., Strasser, U., Verseghy, D., Yamazaki, T., and Yang, Z.-L.: Validation of the energy budget of an alpine snowpack simulated by several snow models (SnowMIP project), Ann. Glaciol., https://doi.org/10.3189/172756404781814825, 2004.

Fortuniak, K.: A slab surface energy balance model (SUEB) and its application to the study on the role of roughness length in forming an
570 urban heat island, Acta Universitatis Wratislaviensis, Studia Geograficzne, 2542, 368–377, 2003.

Fujimoto, A., Tokunaga, R., Kiriishi, M., Kawabata, Y., Takahashi, N., Ishida, T., and Fukuhara, T.: A road surface freezing model using heat, water and salt balance and its validation by field experiments, Cold Regions Science and Technology, 106-107, 1–10, https://doi.org/10.1016/j.coldregions.2014.06.001, 2014.

Giudici, H., Klein-Paste, A., and Wåhlin, J.: Influence of NaCl Aqueous Solution on Compacted Snow: Field Investigation, J. Cold Reg.
575 Eng., 34, https://doi.org/10.1061/(ASCE)CR.1943-5495.0000195, 2019.

Hersbach, H., Bell, B., Berrisford, P., Hirahara, S., Horányi, A., Muñoz-Sabater, J., Nicolas, J., Peubey, C., Radu, R., Schepers, D., Simmons, A., Soci, C., Abdalla, S., Abellan, X., Balsamo, G., Bechtold, P., Biavati, G., Bidlot, J., Bonavita, M., De Chiara, G., Dahlgren, P., Dee, D., Diamantakis, M., Dragani, R., Flemming, J., Forbes, R., Fuentes, M., Geer, A., Haimberger, L., Healy, S., Hogan, R. J., Hólm, E., Janisková, M., Keeley, S., Laloyaux, P., Lopez, P., Lupu, C., Radnoti, G., de Rosnay, P., Rozum, I., Vamborg, F., Villaume, S., and Thépaut,
580 J.-N.: The ERA5 global reanalysis, Q. J. R. Meteorolog. Soc., 146, 1999–2049, https://doi.org/10.1002/qj.3803, 2020.

Järvi, L., Grimmond, C. S. B., Taka, M., Nordbo, A., Setälä, H., and Strachan, I. B.: Development of the Surface Urban Energy and Water Balance Scheme (SUEWS) for cold climate cities, Geosci Model Dev, 7, 1691–1711, https://doi.org/10.5194/gmd-7-1691-2014, 2014.

Kangas, M., Heikinheimo, M., and Hippi, M.: RoadSurf: a modelling system for predicting road weather and road surface conditions, Meteorol Appl, 22, 544–553, https://doi.org/10.1002/met.1486, 2015.

585 Karsisto, V. and Horttanainen, M.: Sky View Factor and Screening Impacts on the Forecast Accuracy of Road Surface Temperatures in Finland, J Appl Meteorol Clim, 62, 121–138, https://doi.org/10.1175/JAMC-D-22-0026.1, 2023.

Karsisto, V. and Lovén, L.: Verification of Road Surface Temperature Forecasts Assimilating Data from Mobile Sensors, Weather and Forecasting, 34, 539 – 558, https://doi.org/10.1175/WAF-D-18-0167.1, 2019.

Karsisto, V., Tijm, S., and Nurmi, P.: Comparing the Performance of Two Road Weather Models in the Netherlands, Wea. Forecasting, 32,
590 991 – 1006, https://doi.org/10.1175/WAF-D-16-0158.1, 2017.

Kršmanc, R., Šajn Slak, A., and Demšarf, J.: Statistical approach for forecasting road surface temperature, Meteorol Appl, 20, 439–446, https://doi.org/doi.org/10.1002/met.1305, 2013.

Lac, C., Chaboureau, J.-P., Masson, V., Pinty, J.-P., Tulet, P., Escobar, J., Leriche, M., Barthe, C., Aouizerats, B., Augros, C., Aumond, P., Auguste, F., Bechtold, P., Berthet, S., Bielli, S., Bosseur, F., Caumont, O., Cohard, J.-M., Colin, J., Couvreux, F., Cuxart, J., Delautier, G.,
595 Dauhut, T., Ducrocq, V., Filippi, J.-B., Gazen, D., Geoffroy, O., Gheusi, F., Honnert, R., Lafore, J.-P., Brossier, C. L., Libois, Q., Lunet, T., Mari, C., Maric, T., Mascart, P., Mogé, M., Molinié, G., Nuissier, O., Pantillon, F., Peyrillé, P., Pergaud, J., Perraud, E., Pianezze, J., Redelsperger, J.-L., Ricard, D., Richard, E., Riette, S., Rodier, Q., Schoetter, R., Seyfried, L., Stein, J., Suhre, K., Taufour, M., Thouron, O., Turner, S., Verrelle, A., Vié, B., Visentin, F., Vionnet, V., and Wautelet, P.: Overview of the Meso-NH model version 5.4 and its applications, Geoscientific Model Development, 11, 1929–1969, https://doi.org/10.5194/gmd-11-1929-2018, 2018.

600 Lemonsu, A., Bélair, S., Mailhot, J., Benjamin, M., Morneau, G., Harvey, B., Chagnon, F., Jean, M., and Voogt, J.: Overview and First Results of the Montreal Urban Snow Experiment 2005, J Appl Meteorol Clim, 47, 59–75, https://doi.org/10.1175/2007jamc1639.1, 2008.

Lemonsu, A., Bélair, S., Mailhot, J., and Leroyer, S.: Evaluation of the Town Energy Balance Model in Cold and Snowy Conditions during the Montreal Urban Snow Experiment 2005, J Appl Meteorol Clim, 49, 346 – 362, https://doi.org/10.1175/2009JAMC2131.1, 2010.

Lemonsu, A., Masson, V., Shashua-Bar, L., Erell, E., and Pearlmutter, D.: Inclusion of vegetation in the Town Energy Balance model for modelling urban green areas, Geoscientific Model Development, 5, 1377–1393, https://doi.org/10.5194/gmd-5-1377-2012, 2012.

Lipson, M., Grimmond, S., Best, M., Chow, W. T. L., Christen, A., Chrysoulakis, N., Coutts, A., Crawford, B., Earl, S., Evans, J., Fortuniak, K., Heusinkveld, B. G., Hong, J.-W., Hong, J., Järvi, L., Jo, S., Kim, Y.-H., Kotthaus, S., Lee, K., Masson, V., McFadden, J. P., Michels, O., Pawlak, W., Roth, M., Sugawara, H., Tapper, N., Velasco, E., and Ward, H. C.: Harmonized gap-filled datasets from 20 urban flux tower sites, Earth System Science Data, 14, 5157–5178, https://doi.org/10.5194/essd-14-5157-2022, 2022.

Lipson, M. J., Grimmond, S., Best, M., Abramowitz, G., Coutts, A., Tapper, N., Baik, J.-J., Beyers, M., Blunn, L., Boussetta, S., Bou-Zeid, E., De Kauwe, M. G., de Munck, C., Demuzere, M., Fatichi, S., Fortuniak, K., Han, B.-S., Hendry, M. A., Kikegawa, Y., Kondo, H., Lee, D.-I., Lee, S.-H., Lemonsu, A., Machado, T., Manoli, G., Martilli, A., Masson, V., McNorton, J., Meili, N., Meyer, D., Nice, K. A., Oleson, K. W., Park, S.-B., Roth, M., Schoetter, R., Simón-Moral, A., Steeneveld, G.-J., Sun, T., Takane, Y., Thatcher, M., Tsiringakis, A., Varentsov, M., Wang, C., Wang, Z.-H., and Pitman, A. J.: Evaluation of 30 urban land surface models in the Urban-PLUMBER project: Phase 1 results, Quarterly Journal of the Royal Meteorological Society, 150, 126–169, https://doi.org/10.1002/qj.4589, 2024.

Masson, V.: A Physically-Based Scheme For The Urban Energy Budget In Atmospheric Models, Boundary Layer Meteorol., 94, 357–397, https://doi.org/10.1023/A:1002463829265, 2000.

Masson, V. and Seity, Y.: Including Atmospheric Layers in Vegetation and Urban Offline Surface Schemes, American Meteorological Society, 48, 1377 – 1397, https://doi.org/10.1175/2009JAMC1866.1, 2009.

Masson, V., Le Moigne, P., Martin, E., Faroux, S., Alias, A., Alkama, R., Belamari, S., Barbu, A., Boone, A., Bouyssel, F., Brousseau, P., Brun, E., Calvet, J.-C., Carrer, D., Decharme, B., Delire, C., Donier, S., Essaouini, K., Gibelin, A.-L., Giordani, H., Habets, F., Jidane, M., Kerdraon, G., Kourzeneva, E., Lafaysse, M., Lafont, S., Lebeaupin Brossier, C., Lemonsu, A., Mahfouf, J.-F., Marguinaud, P., Mokhtari, M., Morin, S., Pigeon, G., Salgado, R., Seity, Y., Taillefer, F., Tanguy, G., Tulet, P., Vincendon, B., Vionnet, V., and Voldoire, A.: The SURFEXv7.2 land and ocean surface platform for coupled or offline simulation of earth surface variables and fluxes, Geoscientific Model Development, 6, 929–960, https://doi.org/10.5194/gmd-6-929-2013, 2013.

Meng, C.: A numerical forecast model for road meteorology, Meteorol. Atmos. Phys., 130, 485–498, https://doi.org/10.1007/s00703-017-0527-8, 2017.

Michaelides, S., Leviäkangas, P., Doll, C., and Heyndrickx, C.: Foreward: EU-funded projects on extreme and high-impact weather challenging European transport systems, https://doi.org/10.1007/s11069-013-1007-1, 2014.

Morin, S., Lejeune, Y., Lesaffre, B., Panel, J.-M., Poncet, D., David, P., and Sudul, M.: An 18-yr long (1993–2011) snow and meteorological dataset from a mid-altitude mountain site (Col de Porte, France, 1325 m alt.) for driving and evaluating snowpack models, Earth System Science Data, 4, 13–21, https://doi.org/10.5194/essd-4-13-2012, 2012.

Muzet, V., Borel, S., and Lassoued, R.: Study of the snow pavement interface: GELCRO project, in: Proc. 10th SIRWEC Conf., Davos, Switzerland, 2000.

Nuijten, A.: Runway temperature prediction, a case study for Oslo Airport, Norway, Cold Regions Science and Technology, 125, 72–84, https://doi.org/10.1016/j.coldregions.2016.02.004, 2016.

Oke, T. R.: Boundary Layer Climates, Methuen, 2nd edn., 1987.

Oleson, K. W., Bonan, G. B., Feddem, J., Vertenstein, M., and Kluzek, E.: Technical Description of an Urban Parameterization for the Community Land Model (CLMU), Tech. Rep. Urban, University Corporation for Atmospheric Research, https://doi.org/10.5065/D6K35RM9, 2010.

Pigeon, G., Moscicki, M. A., Voogt, J. A., and Masson, V.: Simulation of fall and winter surface energy balance over a dense urban area using the TEB scheme, Meteorology and Atmospheric Physics, 102, 159–171, https://doi.org/10.1007/s00703-008-0320-9, 2008.

Pu, Z., Liu, C., Shi, X., Cui, Z., and Wang, Y.: Road surface friction prediction using long short-term memory neural network based on historical data, J Intell Transport S, 26, 34–45, https://doi.org/10.1080/15472450.2020.1780922, 2022.

Qin, Y., Zhang, X., Tan, K., and Wang, J.: A review on the influencing factors of pavement surface temperature, Environ Sci Pollut R, 29, 67 659–67 674, https://doi.org/10.1007/s11356-022-22295-3, 2022.

Qiu, X., Hong, H., Xu, W., Yang, Q., and Xiao, S.: Surface Temperature Prediction of Asphalt Pavement Based on GBDT, IOP Conf. Ser.: Mater. Sci. Eng., 758, 012 031, https://doi.org/10.1088/1757-899X/758/1/012031, 2020.

Sherif, A. and Hassan, Y.: Modelling pavement temperature for winter maintenance operations, Can. J. Civ. Eng., 31, 369–378, https://doi.org/10.1139/l03-107, 2011.

Suher-Carthy, M., Lagelouze, T., Hidalgo, J., Schoetter, R., Touati, N., Jougla, R., and Masson, V.: Urban heat island intensity maps and local weather types description for a 45 French urban agglomerations dataset obtained from atmopsheric numerical simulations, Data in Brief, 50, 109 437, https://doi.org/10.1016/j.dib.2023.109437, 2023.

Takasaki, Y., Saldana, M., Ito, J., and Sano, K.: Development of a method for estimating road surface condition in winter using random forest, Asian Transport Studies, 8, 100 077, https://doi.org/10.1016/j.eastsj.2022.100077, 2022.

Vajda, A., Tuomenvirta, H., Juga, I., Nurmi, P., Jokinen, P., and Rauhala, J.: Severe weather affecting European transport systems: the identification, classification and frequencies of events, Nat Hazards, 72, https://doi.org/10.1007/s11069-013-0895-4, 2013.

Vionnet, V., Brun, E., Morin, S., Boone, A., Faroux, S., Moigne, P. L., Martin, E., and Willemet, J.-M.: The detailed snowpack scheme Crocus and its implementation in SURFEX v7.2, Geosci Model Dev, https://doi.org/10.5194/gmd-5-773-2012, 2012.

Yin, Z., Hadzimustafic, J., Kann, A., and Wang, Y.: On statistical nowcasting of road surface temperature, Meteorological Applications, 26, 1–13, https://doi.org/10.1002/met.1729, 2019.